9th European Workshop on Structural Health Monitoring
July 10-13, 2018, Manchester, United Kingdom

A Bayesian time-of-flight estimation for ultrasonic damage detection

S. Cantero-Chinchilla[1,3], J. Chiachío-Ruano[2], M. Chiachío-Ruano[2], A. Jones[1], Y. Essa[3], and F. Martin De La Escalera[3]

[1] Institute for Aerospace Technology & The Composites Group, The University of Nottingham, NG7 2RD, United Kingdom, Sergio.CanteroChinchilla1@nottingham.ac.uk, Arthur.Jones@nottingham.ac.uk
[2] Resilience Engineering Research Group, The University of Nottingham, NG7 2RD, United Kingdom, Juan.Chiachio-Ruano@nottingham.ac.uk, Manuel.Chiachio-Ruano1@nottingham.ac.uk
[3] Aernnova Engineering Division S.A., Madrid, 28034, Spain, Sergio.Cantero@aernnova.com, Yasser.Essa@aernnova.com, Federico.Martindelaescalera@aernnova.com

Abstract

SHM methods for damage detection and localisation in plate-like structures have typically relied on post-processing of ultrasonic guided waves (GWs) features. The time-of-flight is one of these features, which has been extensively used by the SHM community. A followed technique to obtain the time of flight is by applying a particular time-frequency (TF) transform to get the frequency and energy content of the wave at each instant of time. From these transforms, the selection of a TF model has typically been based on experience, or simply based on minimising the computational cost. In this paper, a full probabilistic method based on the Bayesian inverse problem (BIP) is originally proposed to obtain the most probable model over a set of candidates. To this end, the problem of TF model selection is addressed using a two-stage BIP: (i) first, the posterior PDF of the dispersion parameter is obtained and then, (ii) the most plausible a posteriori value is introduced in the likelihood function to estimate the most evident TF model. The results have revealed the efficiency of the proposed methodology in automatically selecting the most suitable TF model for a relevant case study. No preference for any particular TF model has been found; the most probable TF model is case specific.

1. Introduction

Post-processing techniques of ultrasonic guided waves (GWs) are massively used for damage reconstruction and SHM in many fields of the engineering. Particularly, the aerospace industry has focused on GW based SHM techniques due to its ability to explore large areas with relatively small attenuation [1]. Potential safety and economical implications in the condition based maintenance can be obtained from the use of these autonomous techniques. In addition, aircrafts have a great number of structual components that are out of visual inspection, and hence the need for techniques that allow the remote and automatic exploration of the health state of a structure is more accentuated in

these applications. When a damaged structure is detected, a higher level of information is typically required for further decision making. Hence, one can decide whether (i) to apply model-based inverse problems to obtain highly detailed damage information from the signal (e.g. the severity of damage) [2] at a considerable computational cost, or (ii) to efficiently find the position of the damage. Regarding (ii), several damage reconstruction techniques have been reported in the literature [1, 3–5]. One common point of all of them is the need of obtaining the time of flight of the scattered signal, as the basis of the reconstruction techniques.

TF representation techniques have been widely used for the time of flight extraction purpose. These techniques are able to provide the energy content of each frequency at each instant of time [6]. Amongst them, it is worth mentioning the Hilbert-Huang transform (HHT), the continuous wavelet transform (CWT), the short-time Fourier transform (STFT) and the Wigner-Ville distribution (WVD) [6–8], as the most commonly used techniques. The usefulness of these transforms in GW based SHM problems have been proven by many authors [9–11]. The selection of one of these methods is typically based on experience or on frequency resolution characteristics. It is important to note that the selection of a suboptimal model may result in biased identification or misidentification. Direct comparisons between different TF techniques have been carried out by some authors [12, 13], showing differences between model outputs and when compared to theoretical results. However, a rigorous comparison between TF models is still missing in the literature.

The question of which TF transform is the most appropriate, given the existence of many similar techniques that provide with the same type of outcome, needs to be addressed. In this paper, Bayesian inverse approach is used to address the issue of uncertainty quantification and model ranking over a set of candidates. Uncertainties coming from (i) material propreties, (ii) noise in the acquisition system, and (iii) systematic uncertainty in the TF model due to the Heisenberg uncertainty principle [6, 14] are taken into account. A two-stage BIP is proposed: (I) to infer the dispersion parameter probability density function (PDF) and (II) to obtain the most plausible model. The proposed approach relies on rigorous probabilistic-logic assumptions for model class selection and as such, it avoids experience-based decisions about the optimal post-processing technique. Here, probability is interpreted as a multi-valued logic that expresses the degree of belief of a proposition conditioned on the given information [15, 16]. Therefore, the degree of belief of the dispersion parameter, and the model choice for time of arrival extraction is quantified.

The paper is organised as follows: Section 1 contains the introduction and motivation. Section 2 shows the TF models used in the proposed model selection problem. Section 3 comprises the probabilistic methodology used to obtain the most evident TF model. Section 4 contains a case study where the methodology is applied. Finally, Section 5 provides concluding remarks.

2. TF models

Amongst the most used TF models, a probabilistic assessment of four of them is proposed in this paper. Particularly, HHT, CWT, STFT, and WVD are investigated here and their basic theoretical foundations are presented in this Section.

2.1. *Hilbert-Huang transform*

The Hilbert transform (HT) as a procedure to obtain the envelope of a guided wave is widely used in SHM [7, 12]. In this sense, for an arbitrary time series, $X(t)$, the HT, $Y(t)$, can be defined as:

$$Y(t) = \frac{1}{\pi} P \int_{-\infty}^{\infty} \frac{X(t')}{t - t'} \, \mathrm{d}t', \tag{1}$$

where P denotes the Cauchy principal value. With this definition, $X(t)$ and $Y(t)$ form a complex conjugate pair, so we can have an analytical signal, $Z(t)$, as:

$$Z(t) = X(t) + \mathrm{i}Y(t) = a(t)e^{\mathrm{i}\theta(t)}, \tag{2}$$

where

$$a(t) = [X^2(t) + Y^2(t)]^{1/2}, \qquad \theta(t) = \arctan\left(\frac{Y(t)}{X(t)}\right). \tag{3}$$

The magnitude $a(t)$ of the analytical signal $Z(t)$ is used as the envelope of the input time series $X(t)$. However, this formulation does not provide information about the energy content for each frequency at each instant of time. Thus, Huang et al. introduced the concept of intrinsic mode functions (IMF) whereby the spectrum is defined after performing the HT over each IMF component as [7]:

$$HHT(t) = \sum_{j=1}^{n} a_j(t) \exp\left(\mathrm{i} \int \omega_j(t) \, \mathrm{d}t\right). \tag{4}$$

Equation 4 represents the amplitude and instantaneous frequency as functions of time. Thus, the TF representation can be obtained, known as Hilbert-Huang transform (HHT).

2.2. *Continuous wavelet transform*

The continuous wavelet transform (CWT) has been used in analysing guided waves due to its good resolution in time and frequency domains. This transform uses TF wavelets to obtain the TF representation of the assessed signal. The CWT of a time series $X(t)$ is defined by [8]:

$$CWT(b,a) = \frac{1}{\sqrt{a}} \int_{-\infty}^{\infty} X(t) \overline{\Psi\left(\frac{t-b}{a}\right)} \mathrm{d}t, \tag{5}$$

where $a > 0$ is the scale factor, b is the time-shift variable, and the overbar indicates the complex conjugate. In Equation 5, $\Psi(t)$ denotes the analysing wavelet [17].

2.3. *Short-time Fourier transform*

Other similar transform to CWT is the short-time Fourier transform (STFT). This technique provides with a TF representation of the signal to be analysed. This is particularly useful when assessing Lamb waves, which has a inherently dispersive nature. The basic idea behind it is to perform Fourier transforms to a moving window in the signal. Thus,

the signal is swept and the frequency spectrum is obtained for each of these overlapping time windows [6, 18]. The STFT of a function $X(t)$ is defined as:

$$STFT(\omega,t) = \frac{1}{2\pi}\int_{-\infty}^{\infty} e^{-\mathrm{i}\omega\tau} X(\tau) h(\tau - t)\mathrm{d}\tau, \tag{6}$$

where $h(t)$ is a window function. The energy density spectrum of an STFT, which is defined by $E(\omega,t) = |S(\omega,t)|^2$, is known as the spectrogram.

2.4. Wigner-Ville Distribution

The Wigner-Ville distribution (WVD) is a Fourier transform with respect to τ of the function $X(t+[\tau/2])\overline{X(t-[\tau/2])}$, which is given by [6]:

$$WVD(\omega,t) = \int_{-\infty}^{\infty} X\left(t+\frac{\tau}{2}\right)\overline{X\left(t-\frac{\tau}{2}\right)} e^{-\mathrm{i}\omega\tau}\mathrm{d}\tau. \tag{7}$$

Which can be seen as a measure of the signal's local time-frequency energy [18]. Amongst the capabilities of the WVD, it is worth mentioning that this transform is able to localise Dirac impulses and sinusoids.

3. Probabilistic methodology

A rigorous probabilistic-logic two-stage model selection BIP is proposed and developed in this Section. First, the stochastic embedding of the TF models introduced above is described. Then, a procedure is proposed to solve the BIP whereby the PDF of the dispersion parameter is obtained. Finally, the TF model Bayesian selection procedure, by which the most plausible model is obtained, is explained.

3.1. Stochastic embedding of TF models

Given a TF model g_j that has a discrete signal $\mathscr{D}^{(k)} \in \mathbb{R}^n$ as input, one can define the time at which the first maximum $\hat{d} \in \mathbb{R}$ is received (time of flight) by the sensor as $\hat{d}_j = g_j^{-1}(\mathscr{D}^{(k)})$. It should be emphasized that each model g is only a representation of the reality [16], and thus $\hat{d}_j$ would be more accurately represented as a stochastic variable as:

$$\hat{d}_j = g_j^{-1}\left(\mathscr{D}^{(k)}\right) + \mathbf{e}, \tag{8}$$

where $\mathbf{e}$ is an error term which measures the discrepancy between the modelled and the measured values for $\hat{d}_j$. This error can be assumed to be modelled as a zero-mean Gaussian distribution with variance σ_e, i.e., $e \sim \mathscr{N}(0,\sigma_e)$. This assumption is supported by the Principle of Maximum Information Entropy (PMIE) [15, 16], which provides a rational way to establish a probability model for the error term $\mathbf{e}$ such that it produces the largest uncertainty (largest Shannon entropy). Then, considering Equation 8, a probabilistic description of the TF model can be obtained as:

$$p\left(\hat{d}_k|\mathscr{M}_j,\sigma_e\right) = \left(2\pi\sigma_e^2\right)^{-\frac{1}{2}} \exp\left(-\frac{1}{2}\left(\frac{\hat{d}_k - g_j^{-1}\left(\mathscr{D}^{(k)}\right)}{\sigma_e}\right)^2\right). \tag{9}$$

Each of these stochastic embedding models conforms a *model class* $\mathscr{M}_j$. These candidate model options are subsequently assessed to obtain the most plausible one within the set $\mathbf{M} = \{\mathscr{M}_1, \ldots, \mathscr{M}_j, \ldots, \mathscr{M}_{N_m}\}$, where N_m is the number of TF models.

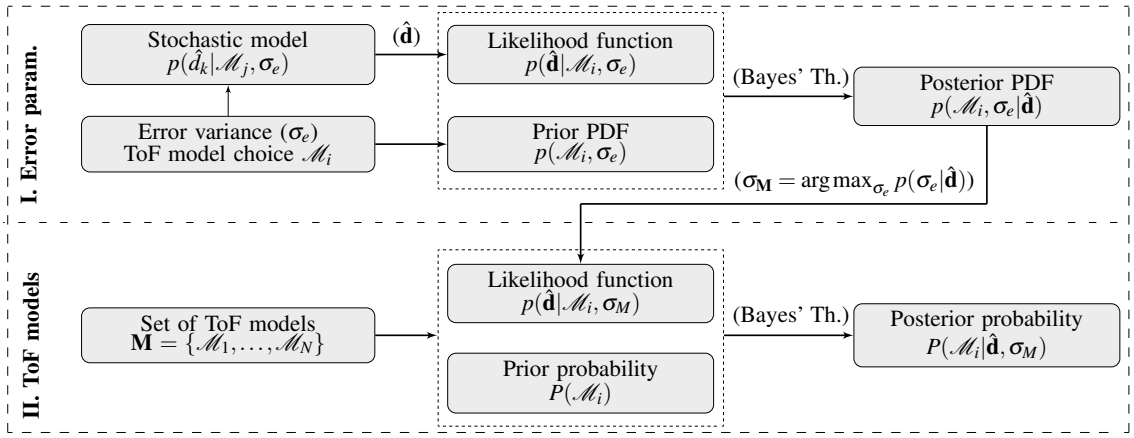

Figure 1: Flowchart of the two-stage model selection BIP. First level (I) estimates the dispersion parameter of the likelihood function by solving a BIP and obtaining the marginal posterior PDF $p(\sigma_e|\hat{\mathbf{d}})$. Second level (II) establishes the probability of each ToF model taking as a constant the error parameter estimated in (I).

3.2. Level I: dispersion parameter estimation

The likelihood function (Equation 9) needs to be completely defined to address the TF models ranking problem. However, Equation 9 is sensitive to the dispersion parameter σ_e, and therefore, the first stage of the BIP is designed to obtain the most plausible value of σ_e. To this end, it is necessary to investigate the joint posterior PDF of the i-th TF model ($\mathscr{M}_i$) and the dispersion parameter σ_e given a set of data $\hat{\mathbf{d}} = \left\{\hat{d}_1 \ldots \hat{d}_N\right\}$, namely $p(\mathscr{M}_i, \sigma_e|\hat{\mathbf{d}})$. From this joint PDF, the marginal posterior $p(\sigma_e|d)$ is derived whereby σ_M is subsequently obtained as a maximum a posteriori (MAP) value of $p(\sigma_e|d)$, as shown in Figure 1. The set of data is obtained as the result of applying the TF models to the Lamb wave signal $\mathscr{D}^{(k)}$. Thus, by using the Bayes' theorem, the posterior PDF is given by:

$$p\left(\mathscr{M}_i, \sigma_e|\hat{\mathbf{d}}\right) \propto p\left(\hat{\mathbf{d}}|\mathscr{M}_i, \sigma_e\right) p\left(\mathscr{M}_i, \sigma_e\right), \tag{10}$$

where $p(\hat{\mathbf{d}}|\mathscr{M}_i, \sigma_e)$ is the likelihood function, which expresses how likely the dataset $\hat{\mathbf{d}}$ is obtained by the stochastic model in Equation 9 if model class $\mathscr{M}_i$ is adopted as shown in Figure 2. This likelihood function can be obtained by substituting the values $\hat{\mathbf{d}}$ as the output of the stochastic model, as:

$$p\left(\hat{\mathbf{d}}|\mathscr{M}_i, \sigma_e\right) = \prod_{\ell=1}^{N} p\left(\hat{d}_\ell|\mathscr{M}_i, \sigma_e\right). \tag{11}$$

The prior information term $p(\mathscr{M}_i, \sigma_e)$ in Equation 10 can be addressed separately assuming the stochastic independence of $\mathscr{M}_i$ and σ_e, as $p(\mathscr{M}_i, \sigma_e) = P(\mathscr{M}_i)p(\sigma_e)$. Therefore, Equation 10 rewrites as:

$$p\left(\mathscr{M}_i, \sigma_e|\hat{\mathbf{d}}\right) \propto \left\{\prod_{\ell=1}^{N} p\left(\hat{d}_\ell|\mathscr{M}_i, \sigma_e\right)\right\} P\left(\mathscr{M}_i\right) p\left(\sigma_e\right). \tag{12}$$

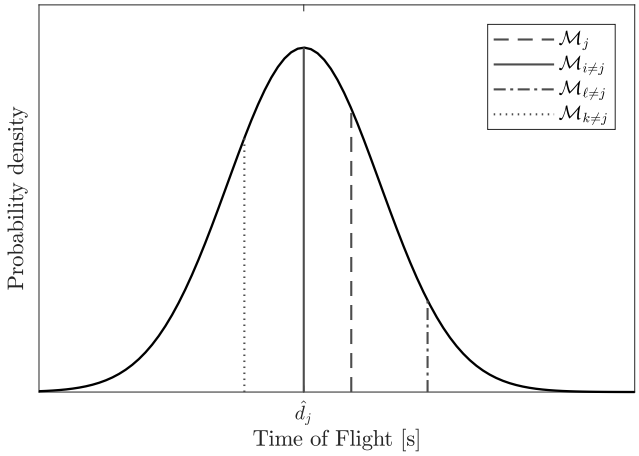

Figure 2: Likelihood function defined in one specific time of flight ($\hat{d}_j$). The other data provided by the rest of TF models are also evaluated in the defined likelihood function $p(\hat{\mathbf{d}}|\mathscr{M}_j, \sigma_e)$.

An updating algorithm is needed to obtain the numerical estimate the posterior PDF of the dispersion parameter σ_e, which is essential for the problem of model selection, as shown in Figure 1. The well-known Metropolis-Hastings (M-H) [19, 20] is adopted due to its efficiency and simplicity for implementation. The marginal posterior PDF of the standard deviation of the dispersion parameter $p(\sigma_e|\hat{\mathbf{d}})$ is obtained, and then the model selection problem (*level II*) can be addressed as depicted in Figure 1. The representative value of the dispersion parameter is selected as the MAP estimate, σ_M , from the marginal posterior PDF $p(\sigma_e|\hat{\mathbf{d}})$ and it is given by:

$$\sigma_M = \arg\max_{\sigma_e} p(\sigma_e|\hat{\mathbf{d}}) = \{\sigma_e | p(\sigma_e|\hat{\mathbf{d}}) = \max_{\sigma'_e} p(\sigma'_e|\hat{\mathbf{d}})\}. \tag{13}$$

3.3. Level II: model selection

The model selection problem can now be addressed by introducing the MAP estimate of the dispersion parameter, σ_M, in the likelihood function as a deterministic value. This is enforced by the asymptotic Laplace's approximation [16] which states that:

$$p\left(\hat{\mathbf{d}}|\mathscr{M}_i\right) \approx p\left(\hat{\mathbf{d}}|\mathscr{M}_i, \sigma_e\right). \tag{14}$$

This approximation is valid if $p(\sigma_e|\hat{\mathbf{d}})$ is globally identifiable, i.e. if the PDF has a unique global maximum value. From this standpoint, the model selection problem can be solved by applying the Bayes' Theorem. Therefore, the plausibility of the i-th TF model $\mathscr{M}_i$ given the set of data $\hat{\mathbf{d}}$ is defined as follows:

$$P\left(\mathscr{M}_i|\hat{\mathbf{d}}, \sigma_M\right) \propto \left\{\prod_{\ell=1}^{N} p\left(\hat{d}_\ell, \sigma_M|\mathscr{M}_i\right)\right\} P\left(\mathscr{M}_i\right). \tag{15}$$

The probability of each TF model can be obtained by evaluating each of these likelihood functions and by multiplying by the prior information. As can be deduced, Equation 15 may be analytically evaluated, since the likelihood function is modelled by a Gaussian distribution and the prior information is known.

4. Case Study

This section describes the case study applied to test the proposed methodology over a set of guided waves numerically acquired through a finite element model (FEM). The models described in Section 2 are then ranked by using the proposed probabilistic methodology, as shown below.

4.1. Numerical model

Ultrasonic guided waves were obtained by making use of an aluminium plate modelled in Abaqus®, inspired by the FEM proposed in [10]. The model represents a 0.3 [m] $\times 0.3$ [m] aluminium plate, which properties are summarised in Table 1. An aluminium alloy 2024-T351 [21], commonly used in aerospace, is selected in this case study. The Abaqus explicit module is used to obtain the transient representation of the ultrasonic guided waves in four arbitrary points of the plate. The origin of the coordinate system is assumed in the center of the plate, where the actuator is placed, i.e $(0,\ 0)$ [m]. The four sensors coordinates are as follows: (i) sensor 1 in $(0,\ 0.1)$ [m], (ii) sensor 2 in $(0.1,\ 0.05)$ [m], (iii) sensor 3 in $(-0.09,\ -0.07)$ [m], and (iv) sensor 4 in $(-0.03,\ -0.12)$ [m].

Table 1: Material properties (aluminium alloy 2024-T351 [21]) used in the Abaqus model.

Young's modulus [GPa]	Poisson's ratio [-]	Density [kg/m^3]	Thickness [mm]
73.1	0.33	2780	2

A uniform square mesh of 1mm element size is used with a S4R shell element type. Free boundary conditions are considered in this model. The load is generated as a sine tone-burst centred at 100 kHz with 5 cycles. The direction of application of this load is normal to the surface of the plate, since the piezoceramic sensors and actuator are not modelled to gain computational efficiency. Then, a hole in square shape was modelled to mimic damage in the plate. The signals acquired in undamaged and damaged conditions are then subtracted to obtain the scattered signals, shown in Figure 3, that carry the damage information. These signals are then the data $\mathscr{D}$ used in the probabilistic methodology to rank the different TF models.

4.2. Model selection results

The signals shown in Figure 3 are introduced in the probabilistic model selection methodology presented in Section 3. As there is no initial guess on the standard deviation of the dispersion parameter, a uniform PDF is selected as prior PDF for all the signals assessed. This standard deviation σ_e parameter is defined by a factor ρ that multiplies the time of arrival, $\hat{d}_j$ as: $\sigma_e = \rho \hat{d}_j$. Thus, the prior PDF is defined as the uniform distribution for $\rho \in (0, 0.5]$.

The obtained posterior PDFs of the standard deviation factor ρ of the selected TF models are depicted in Figure 4. Then, the value of the maximum pseudo-posterior probability is selected to be introduced in *level II* of the methodology as presented in Section 3.3. To do so, some analytical PDFs are fitted to the PDFs to address the search of the standard deviation factor that holds the maximum pseudo-posterior plausibility. As observed in

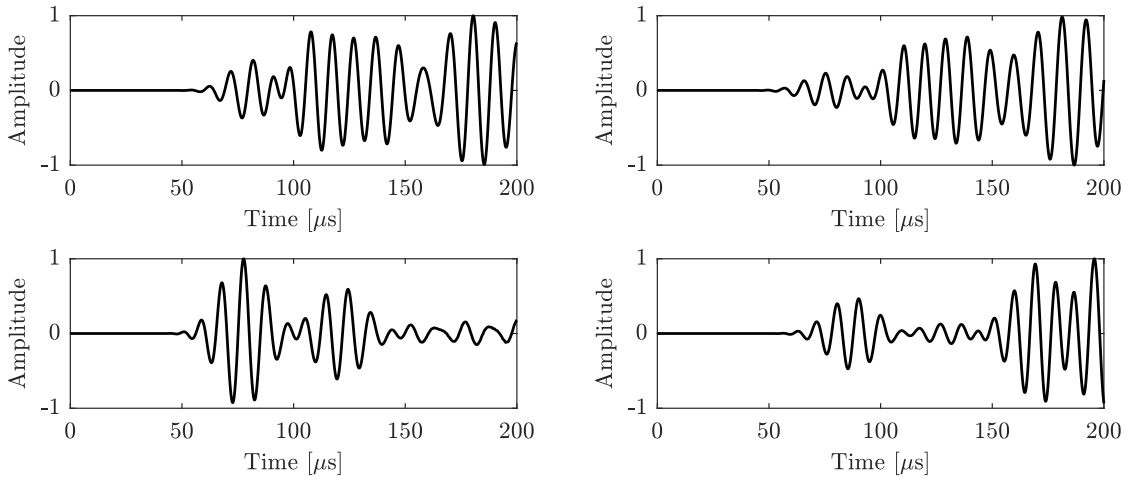

Figure 3: Scattered signals of the damaged structure obtained in the FEM. Signal 1: top left figure. Signal 2: top right figure. Signal: bottom left figure. Signal 4: bottom right figure. The numbering corresponds to the sensors order.

Table 2: Standard deviation (σ_M) and standard deviation factor (ρ_M) of the dispersion parameter per model and signal in the *level I* of the proposed methodology.

		Model: HHT	Model: CWT	Model: STFT	Model: WVD
Signal 1	ρ_M	0.0110	0.0115	0.0178	0.0173
	σ_M	6.1719e-7	6.4064e-7	1.0102e-6	9.5510e-7
Signal 2	ρ_M	0.0223	0.0140	0.0148	0.0219
	σ_M	1.1888e-6	7.3652e-7	7.7034e-7	1.1281e-6
Signal 3	ρ_M	0.0032	0.0037	0.0060	0.0050
	σ_M	1.6739e-7	1.9317e-7	3.1530e-7	2.6055e-7
Signal 4	ρ_M	0.0027	0.0045	0.0049	0.0026
	σ_M	1.6769e-7	2.8038e-7	3.0307e-7	1.6768e-7

Figure 4, the best PDF that fits the posterior PDFs is the *generalised extreme values* distribution [22]. The MAP value is selected and therefore the standard deviation factor ρ_M is obtained and presented in Table 2. Then, the standard deviation σ_e that corresponds to the selected factors ρ are obtained and shown in Table 2. Finally, these values are introduced in the *level II* to obtain the most probable TF model.

The pseudo-posterior probabilities used to rank the TF models for each signal are shown in Table 3. Based on the results, HHT results to be the most evident TF model for signals 1, 3 and 4, whereas CWT is the most plausible in the case of signal 2. It is worth mentioning that for signal 4, both HHT and WVD holds a very similar plausibility (1.2252e+24 and 1.2251e+24 respectively). This can be explained since both TF models obtained very similar ToA (6.2106e−5 and 6.2103e−5 respectively), as shown in Table 3.

5. Conclusions

A two-stage Bayesian methodology that ranks TF models to rigorously obtain the most plausible one is presented in this paper. This methodology addresses the problem while

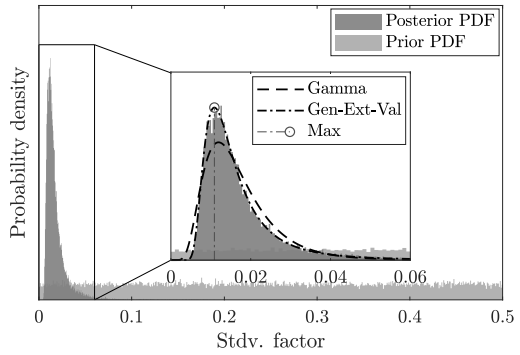

(a) Model: HHT; Signal: 1

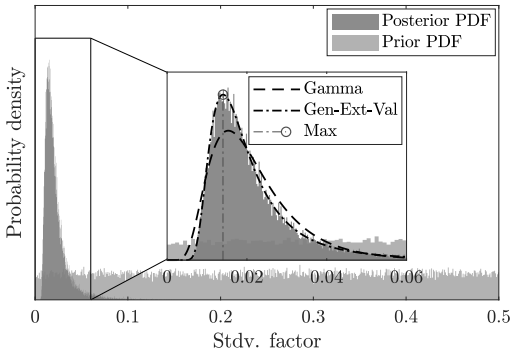

(b) Model: CWT; Signal: 2

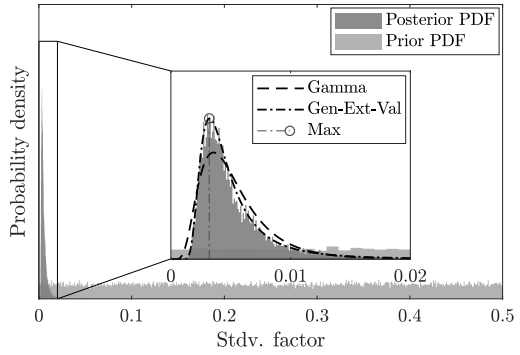

(c) Model: HHT; Signal: 3

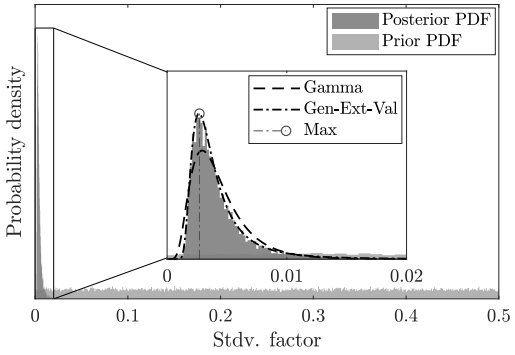

(d) Model: HHT; Signal: 4

Figure 4: Marginal prior $p(\sigma_e)$ and posterior PDFs $p(\sigma_e|\hat{\mathbf{d}})$ of the selected TF models for each signal.

Table 3: Pseudo-posterior probability ($p(\mathscr{M}_j|\hat{\mathbf{d}})$) and time of arrival ($\hat{d}_j$) in the *level II* of the proposed methodology.

		Model: HHT	Model: CWT	Model: STFT	Model: WVD
Signal 1	$p(\mathscr{M}_j\|\hat{\mathbf{d}})$	**7.1162e+21**	6.0796e+21	9.1050e+20	1.1568e+21
	$\hat{d}_j$ [s]	**5.6108e-5**	5.5708e-5	5.6750e-5	5.5208e-5
Signal 2	$p(\mathscr{M}_j\|\hat{\mathbf{d}})$	4.8418e+20	**3.3713e+21**	2.8439e+21	6.0744e+20
	$\hat{d}_j$ [s]	5.3309e-5	**5.2609e-5**	5.2050e-5	5.1509e-5
Signal 3	$p(\mathscr{M}_j\|\hat{\mathbf{d}})$	**1.1726e+24**	7.3260e+23	1.0021e+23	2.2705e+23
	$\hat{d}_j$ [s]	**5.2309e-5**	5.2209e-5	5.2550e-5	5.2109e-5
Signal 4	$p(\mathscr{M}_j\|\hat{\mathbf{d}})$	**1.2252e+24**	1.6406e+23	1.1844e+23	**1.2251e+24**
	$\hat{d}_j$ [s]	**6.2106e-5**	6.2306e-5	6.1850e-5	**6.2103e-5**

accounting for the several sources of uncertainty, therefore, providing a rigorous tool to obtain the time of arrival for damage reconstruction. The effectiveness of the method is shown using a case study with four different guided wave scatter signals. Overall, no preference in TF model selection is observed, thus showing the importance of considering a model selection problem before facing an ultrasound-based damage identification problem.

Acknowledgements

This paper is part of a project that has received funding from the European Union's Horizon 2020 research and innovation programme under the Marie Skłodowska-Curie grant agreement No 721455.

References

1. Z. Su, L. Ye, and Y. Lu, "Guided Lamb waves for identification of damage in composite structures: A review," Journal of sound and vibration, vol. 295, no. 3-5, pp. 753–780, 2006.

2. J. Chiachío, N. Bochud, M. Chiachío, S. Cantero, and G. Rus, "A multilevel Bayesian method for ultrasound-based damage identification in composite laminates," Mechanical Systems and Signal Processing, vol. 88, pp. 462–477, 2017.

3. C. H. Wang, J. T. Rose, and F.-K. Chang, "A synthetic time-reversal imaging method for structural health monitoring," Smart materials and structures, vol. 13, no. 2, p. 415, 2004.

4. J. E. Michaels and T. E. Michaels, "Guided wave signal processing and image fusion for in situ damage localization in plates," Wave motion, vol. 44, no. 6, pp. 482–492, 2007.

5. J. E. Michaels, A. J. Croxford, and P. D. Wilcox, "Imaging algorithms for locating damage via in situ ultrasonic sensors," in Sensors Applications Symposium, 2008. SAS 2008. IEEE, pp. 63–67, IEEE, 2008.

6. L. Cohen, "Time-frequency Analysis: Theory and Applications". Upper Saddle River, NJ, USA: Prentice-Hall, Inc., 1995.

7. N. E. Huang, Z. Shen, S. R. Long, M. C. Wu, H. H. Shih, Q. Zheng, N.-C. Yen, C. C. Tung, and H. H. Liu, "The empirical mode decomposition and the Hilbert spectrum for nonlinear and non-stationary time series analysis," in Proceedings of the Royal Society of London A: mathematical, physical and engineering sciences, vol. 454, pp. 903–995, The Royal Society, 1998.

8. C. K. Chui, "An Introduction to Wavelets". San Diego, CA, USA: Academic Press Professional, Inc., 1992.

9. C. Fendzi, N. Mechbal, M. Rebillat, M. Guskov, and G. Coffignal, "A general Bayesian framework for ellipse-based and hyperbola-based damage localization in anisotropic composite plates," Journal of Intelligent Material Systems and Structures, vol. 27, no. 3, pp. 350–374, 2016.

10. G. Yan, "A Bayesian approach for damage localization in plate-like structures using Lamb waves," Smart Materials and Structures, vol. 22, no. 3, p. 035012, 2013.

11. M. S. Salmanpour, Z. Sharif Khodaei, and M. Aliabadi, "Impact damage localisation with piezoelectric sensors under operational and environmental conditions," Sensors, vol. 17, no. 5, p. 1178, 2017.

12. B. Xu, L. Yu, and V. Giurgiutiu, "Advanced methods for time-of-flight estimation with application to lamb wave structural health monitoring," in Proc. International Workshop on SHM, pp. 1202–1209, 2009.

13. L. Peralta, X. Cai, P. Laugier, and Q. Grimal, "A critical assessment of the in-vitro measurement of cortical bone stiffness with ultrasound," Ultrasonics, vol. 80, pp. 119–126, 2017.

14. E. D. Niri and S. Salamone, "A probabilistic framework for acoustic emission source localization in plate-like structures," Smart Materials and Structures, vol. 21, no. 3, p. 035009, 2012.

15. E. T. Jaynes, "Information theory and statistical mechanics," Physical review, vol. 106, no. 4, p. 620, 1957.

16. J. L. Beck, "Bayesian system identification based on probability logic," Structural Control and Health Monitoring, vol. 17, no. 7, pp. 825–847, 2010.

17. H. Jeong and Y.-S. Jang, "Wavelet analysis of plate wave propagation in composite laminates," Composite Structures, vol. 49, no. 4, pp. 443–450, 2000.

18. M. Niethammer, L. J. Jacobs, J. Qu, and J. Jarzynski, "Time-frequency representations of Lamb waves," The Journal of the Acoustical Society of America, vol. 109, no. 5, pp. 1841–1847, 2001.

19. N. Metropolis, A. W. Rosenbluth, M. N. Rosenbluth, A. H. Teller, and E. Teller, "Equation of state calculations by fast computing machines," The journal of chemical physics, vol. 21, no. 6, pp. 1087–1092, 1953.

20. W. K. Hastings, "Monte Carlo sampling methods using Markov chains and their applications," Biometrika, vol. 57, no. 1, pp. 97–109, 1970.

21. T. Dursun and C. Soutis, "Recent developments in advanced aircraft aluminium alloys," Materials & Design (1980-2015), vol. 56, pp. 862–871, 2014.

22. S. Kotz and S. Nadarajah, "Extreme value distributions: theory and applications". World Scientific, 2000.